Suplemento de la Revista Mexicana de Física **4** 021125 (2023) 1–5

Minimal center-of-mass energy required for QGP formation in pp and AA collisions

D. Rosales Herrera

Facultad de Ciencias Físico Matemáticas, Benemérita Universidad Autónoma de Puebla, Apartado Postal 165, 72000 Puebla, Puebla, México.

A. Fernández Téllez

Facultad de Ciencias Físico Matemáticas, Benemérita Universidad Autónoma de Puebla, Apartado Postal 165, 72000 Puebla, Puebla, México.

J. E. Ramírez

Centro de Agroecología, Instituto de Ciencias, Benemérita Universidad Autónoma de Puebla, Apartado Postal 165, 72000 Puebla, Puebla, México.
e-mail: jhony.ramirezcancino@viep.com.mx

Received 14 May 2023; accepted 20 July 2023

We discuss the conditions for QGP formation under the Color String Percolation Model (CSPM). Since the observables in the percolation theory are sensitive to the system size, we expect that the finite size effects make a relevant contribution to the estimation of the CSPM phenomenology, such as the transition temperature or the center of mass energy needed for the QGP formation. We observe that pp collisions (small systems) require around 20 times bigger center of mass energy than heavy ion collisions. Our results are consistent with the energy of those experiments in which the QGP has been observed.

Keywords: High energy physics; percolation; center-of-mass energy.

DOI: https://doi.org/10.31349/SuplRevMexFis.4.021125

1. Introduction

In high energy physics experiments, such as those performed at RHIC [1–3] and LHC [4–6], two projectiles (protons or heavy nuclei) moving at velocities close to the speed of light collide. Moments before the collision, due to the Lorentz contraction, these projectiles resemble two thin disks from which color flux tubes emanate. On the transverse plane, these objects can be modeled as randomly distributed disks of radius $r_0 \sim 0.2 - 0.3$ fm, called color strings.

The fundamental interaction between the color strings is given by their overlapping promoting the formation of clusters in the transverse plane, in a similar picture as the two-dimensional continuum percolation theory. As the center-of-mass energy $\sqrt{s}$ or the number of nucleons of the projectiles increases, the number of color strings in the system raises until reaching a critical density, as we depicted in Fig. 1. At this point, a giant cluster of color strings emerges, as Fig. 1c) shown. In the percolation context, it is possible to associate the formation of the percolating cluster with the quarks confined-unconfined state, called Quark-Gluon Plasma (QGP), which has been experimentally observed in AuAu collisions at RHIC and PbPb at LHC.

This phenomenon can be well described by the Color String Percolation Model (CSPM) [7–10], which is the implementation of the two-dimensional continuous percolation model with disks and the theory of quantum chromodynamics.

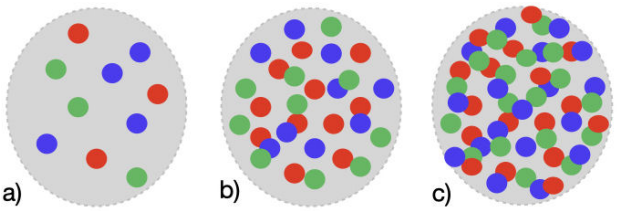

FIGURE 1. a) Isolated color strings, b) clusters formation, c) emerge of the spanning cluster associated to the QGP formation.

The rest of this manuscript is organized as follows. In Sec. 2, we discuss the observables defined in the CSPM, for example, the multiplicity, the average of the transverse momentum squared, and temperature, among others. Section 3 contains the discussion of the simulation method and data analysis. In Sec. 4, we discuss the finite size effects on the CSPM. In particular, we derive the minimal center of mass energy required for QGP formation as a function of the nucleus number. We summarize our findings in a phase diagram that describes the QGP formation together with different pp and AA collision experiments. Finally, Sec. 5 contains our conclusions.

2. Observables in the CSPM

The interaction of the color strings through their overlap gives rise to several color sources with different color field

strengths [11, 12], which must satisfy the vectorial sum of color charges. For example, in a cluster of n color strings, we can identify the color source with area $S_n^{(i)}$ where i counts the number of strings that overlap there. Thus, in such region, the color charge is $Q_n^{(i)} = \sqrt{i}Q_1\left(\frac{S_n^{(i)}}{S_1}\right)$ because the individual color strings may be arbitrarily oriented with respect to each other. Note that the resulting color charge is lower than the linear superposition of the color fields iQ_1 [13–15]. Because of that, it is expected a reduction in the multiplicity of the particles produced, and an increase of the mean transverse momentum due to an increase in the string tension [11, 12]. Therefore, for a cluster of n color strings

$$\mu_n = \sqrt{\frac{nS_n}{S_1}}\mu_1, \tag{1}$$

$$\langle p_T^2\rangle = \sqrt{\frac{nS_1}{S_n}}\langle p_T^2\rangle_1, \tag{2}$$

where S_n is the area covered by the cluster. Notice that Eqs. (1) and (2) are between the extreme cases of minimal and maximum overlap [16]. This means that for n strings touching only at their borders $S_n = nS_1$, then the total multiplicity and average transverse momentum squared are $\mu_n = n\mu_1$ and $\langle p_T^2\rangle = \langle p_T^2\rangle_1$, respectively. On the other hand, when the n strings totally overlap $S_n = S_1$, and hence $\mu_n = \sqrt{n}\mu_1$ and $\langle p_T^2\rangle = \sqrt{n}\langle p_T^2\rangle_1$. In any case, the multiplication of both quantities can be understood as a conservation law [17, 18].

In the CSPM, it is assumed that N color strings are uniformly distributed in the transverse plane to the collision. In this way, the fluctuations of the string density $\eta = NS_1/S$ are described by a Poisson distribution with average η. Therefore, in the thermodynamic limit, the fraction of covered area by the color strings S_n/S corresponds to [19, 20]

$$\sum_{n=1} \text{Poisson}_n = 1 - e^{-\eta}. \tag{3}$$

Thus, by considering the fluctuations in the number of color strings at a fixed value of η, Eq.(1) weighted by μ_1 becomes

$$\frac{\mu}{\mu_1} = \frac{\langle\sqrt{n}\rangle}{S_1}S = N\frac{\langle\sqrt{n}\rangle}{\eta}, \tag{4}$$

where $\langle\sqrt{n}\rangle/\eta$ is a damping factor on multiplicity between 0 and 1 [15, 17]. Then, in the thermodynamic limit approximation, it is found

$$F(\eta) = \frac{\langle\sqrt{n}\rangle}{\eta} = \sqrt{\frac{1-e^{-\eta}}{\eta}}. \tag{5}$$

Since the purpose of this work is to measure the finite size effects on the observables of the CSPM, we will hold the definition $F(\eta) = \sqrt{\frac{\phi(\eta)}{\eta}}$, where $\phi(\eta)$ is the area covered by the color strings [20].

Finally, through the color suppression factor $F(\eta)$, it is possible to estimate the multiplicity and the mean transverse momentum, which in the CSPM are given by

$$\mu = N\mu_1 F(\eta), \tag{6}$$

$$\langle p_T^2\rangle = \frac{\langle p_T^2\rangle_1}{F(\eta)}, \tag{7}$$

respectively.

2.1. Temperature in the CSPM

In the Color String Percolation Model, it is possible to define a temperature for the color string systems through the Schwinger mechanism, which dictates the transverse momentum distribution, given by

$$\frac{dN}{dp_T^2} \sim e^{-\pi p_T^2/x^2}, \tag{8}$$

where $\langle x^2\rangle$ is the mean tension string. In Ref. [17] it is assumed that such tension fluctuates according to a Gaussian distribution

$$G(x) = \frac{1}{\sqrt{2\pi\langle x^2\rangle}}e^{-\frac{x^2}{2\langle x^2\rangle}}. \tag{9}$$

The convolution of (8) with the Gaussian fluctuations transforms the Schwinger mechanism into a thermal distribution as follows

$$\frac{dN}{dp_T^2} \sim e^{-p_T\beta}, \tag{10}$$

with $\beta = \sqrt{\frac{2\pi}{\langle x^2\rangle}}$. Notice the similarity of (10) to the Boltzmann distribution, where we directly identify $T = 1/\beta$ as the temperature of color string systems. This temperature can be extracted from the analysis of the transverse momentum spectra, but its fundamental role is to connect the CSPM with experimental data.

Therefore, by calculating $\langle p_T^2\rangle$ through the normalized Schwinger mechanism and comparing with Eq. (7) it is possible to define a temperature

$$T = \sqrt{\frac{\langle p_T^2\rangle_1}{2F(\eta)}}, \tag{11}$$

for the CSPM that we can relate to η and the cluster formation.

3. Methodology

It is well-accepted that the emergence of the spanning cluster of color strings marks the onset of the QGP formation [8, 10, 21, 22]. Thus, it is necessary to analyze the behavior of the CSPM observables at the percolation threshold, which can be done by computer simulation. For this purpose, we adopt the Mertens-Moore simulation scheme [23]. In our implementation, disks are added one by one and uniformly randomly placed on a square of side L until the spanning cluster emerges. At this step, the number of disks added is stored. Using the data obtained from 10^5 simulations, we compute the probabilities f_n and $\mathcal{F}_L(n) = \sum_{k=1}^{n} f_k$ of observing the

emergence of the spanning cluster after adding exactly and at most n disks, respectively. Then, the percolation probability $P_L(\eta)$ is estimated as following

$$P_L(\eta) = \sum_{n=0}^{\infty} \mathcal{F}_L(n)\text{Poisson}(\lambda)_n, \tag{12}$$

where Poisson distribution with $\lambda = \eta L^2/\pi r_0^2$ describes the spatial allocation of the disks' centers and its fluctuations when a system is filled with a fixed density. Notice that in Eq. (12) the calculation of $n!$ for large values of n can bring numerical difficulties, so the quotients $\lambda^n/n!$ are replacing by Poisson weight w_n, which are estimated with the recursive form discussed in Ref. [23].

Thus, percolation probability is rewritten as

$$P_L(\eta) = e^{-\lambda} \sum_{n=N_{\text{mÃ¡n}}}^{N_{\text{mÃ¡x}}} \mathbf{F}_L(N) w_n \Bigg/ \sum_{n=N_{\text{mÃ¡n}}}^{N_{\text{mÃ¡x}}} w_n \ , \tag{13}$$

where the upper and lower limit of summation has been bounded by using the 5σ criterion. It is observed that the simulation data exhibit a sigmoid shape transition, which can be fitted by the function

$$P_L(\eta) = \frac{1}{2}\left(1 + \tanh\left(\frac{\eta - \eta_{cL}}{\Delta_L}\right)\right), \tag{14}$$

where η_{cL} is the estimated percolation threshold for a system of size L, and Δ_L corresponds to the width of the transition region in which the percolation probability goes from 0 to 1 [18, 20]. We found the following scaling relations for η_{cL} and Δ_L

$$\Delta_L \propto L^{-1/\nu}, \tag{15}$$

$$\eta_{cL} - \eta_c \propto L^{-2/\nu}, \tag{16}$$

where $\nu = 4/3$ is the critical exponent associated with the length correlation. Notice that Eqs. (15) and (16) are in agreement with those scaling relations reported in the literature for percolation systems [24]. Moreover, by fitting Eq. (16) our estimation of the percolation threshold in the thermodynamic limit is $\eta_c = 1.1279(1)$, which is in good agreement with the most precise determination of η_c for 2D-continuum percolation systems of fully overlapped disks [23].

The observables of interest in CSPM can be estimated at η_{cL} by using Eq. (13), where its estimations after adding exact n-color strings are required. To avoid divergence and dependence on undetermined parameters on the multiplicity, mean transverse momentum and temperature, it is convenient to define the following quantities

$$\mathcal{M} = \frac{M}{M_1} = NF(\eta), \tag{17}$$

$$\mathcal{P} = \frac{\langle p_T^2\rangle}{\langle p_T^2\rangle_1} = \frac{1}{F(\eta)}, \tag{18}$$

$$T^* = \frac{T(\eta)}{\sqrt{\langle p_T^2\rangle_1}} = \frac{1}{\sqrt{2F(\eta)}}, \tag{19}$$

TABLE I. Critical values and exponents of the scaling law (20) for the observables of interest.

Observable X	X_c	Y
η	1.1279(1)	-1.5
ϕ	0.6757(7)	-2
F	0.7742(1)	-1.3
$\mathcal{M}$	0.8731(6)	-1.66
$\mathcal{P}$	1.2917(2)	-1.33
T^*	0.80365(8)	-1.32

where $\mathcal{M}$ is a dimensionless multiplicity density, $\mathcal{P}$ is a dimensionless mean transverse momentum and T^* is a dimensionless temperature, respectively. In Eq. (17), $M = \mu/L^2$, and $M_1 = \mu_1/L^2$ is a constant.

By analyzing the behavior of all the observables at the percolation threshold as a function of L, we found that they scale in the forms of power-laws as follows

$$X_{cL} - X_c \propto L^Y, \tag{20}$$

where X_{cL} is the estimation of the observable as a function of L, X_c is the corresponding estimation in the thermodynamic limit, and Y is an exponent. In Table I, we summarize the value of the parameters X_c (determination of the critical value in the thermodynamic limit) and its corresponding exponent Y of Eq. (20) for each observable.

4. Results

4.1. Finite Size Effects

In the CSPM are expected finite size effects since simulations on percolation theory depend on the system size. This implies perceptible differences in the CSPM observables for pp collisions than AA ones. To describe a symmetric central collision in terms of the model we enclose the impact surface S in a square of side

$$L = \frac{R_A}{r_0} = \frac{A_M^{1/3} r_0^*}{r_0}, \tag{21}$$

where R_A is the atomic radius, A_M the nucleon number, and $r_0^* = 1.25$ fm a constant. Then, by substituting Eq.(21) in the scaling relation (20), the observables can be related to a specific projectiles through $X_{cL} - X_c \propto 5A_M^{Y/3}$. In Fig. 2 we show the estimations of the transition temperature T^* associated to the QGP formation for pp and AA collisions. Notice that T^* is higher for small systems, which implies higher center-of-mass energy $\sqrt{s}$.

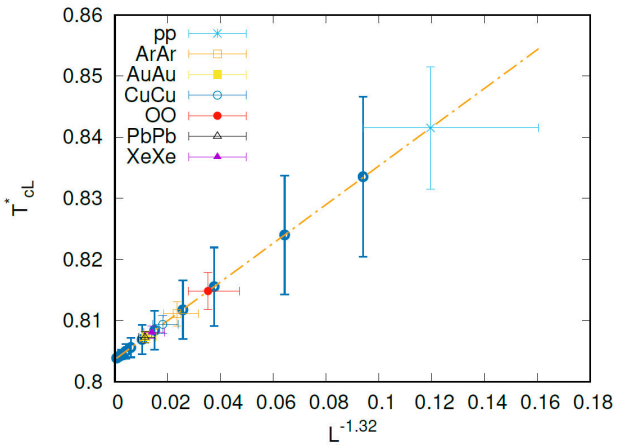

FIGURE 2. Dimensionless transition temperature for pp and AA collisions. Figures are simulation data.

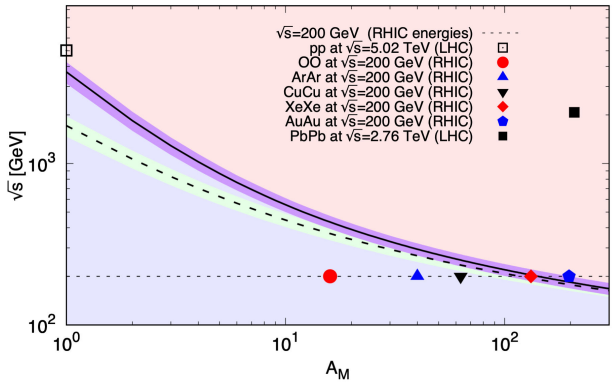

FIGURE 3. Phase diagram of the Quark-Gluon Plasma formation, where figures correspond to collisions at different center-of-mass energies.

4.2. String density and center-of-mass energy

It is possible to relate η and $\sqrt{s}$ for a particular system by determining the number of produced color strings in the collision [25], which can be rewritten as a filling factor by multiplying by the ratio between the area of a single string and the surface of the transverse area. Thus, we obtain [26]

$$\eta^{pp}(\sqrt{s}) = \frac{\pi}{25}\left[2 + 4\left(\frac{r_0}{R_p}\right)^2\left(\frac{\sqrt{s}}{m_p}\right)^{2\lambda}\right], \qquad (22)$$

for pp collisions, and

$$\eta^{AA}(\sqrt{s}) = \eta^{pp}(\sqrt{s})A_M^{\alpha(\sqrt{s})}, \qquad (23)$$

for AA collisions, with

$$\alpha(\sqrt{s}) = \frac{1}{3}\left[1 - \frac{1}{1+\ln(\sqrt{s/s_0}+1)}\right], \qquad (24)$$

where R_p is the proton radius, m_p the proton mass, and $\sqrt{s_0} = 245(29)$ GeV found in the fit of experimental data [25, 26].

The minimal center-of-mass energy required for QGP formation is estimated by solving the equation $\eta^{AA} = \eta_{cL}$ since the onset of the QGP formation is associated with the emergence of the spanning cluster. By using η_{cL} instead of η_c, we assure to take into account the finite size effects on the percolation threshold. Figure 3 we show our results on the estimation of the minimal center of mass required for QGP formation as a function of the nucleon number (solid line). We also plot the corresponding estimation when $\eta^{AA} = \eta_c$, *i.e.*, without considering the finite size effects. We found relevant deviation for small systems as pp collision, where the ratio is around 0.5. However, this difference vanishes as A_M increases because they correspond to large percolating systems.

4.3. QGP phase diagram

The most important result presented in this work is the QGP phase diagram in the space parameters $\sqrt{s}$ - A_M, where $\sqrt{s} = 200$ GeV is the RHIC energy. In Fig. 3 solid line represents the critical curve for minimal center-of-mass energy when finite size effects are taking account, splitting the regions where QGP may (red shaded region) or may not (blue shaded region) be observed. Dashed line correspond to the $\sqrt{s}$ minimal values when we assume that the spanning cluster of color strings in each collision emerges at the percolation threshold in the thermodynamic limit η_c. Purple and green regions are related to the errors in such estimations.

Notice that the obtained estimations are consistent with the data experiment, in particular for AuAu ($\sqrt{s} = 200$ GeV) and PbPb ($\sqrt{s} = 2.76$ TeV) collisions at RHIC and LHC respectively, in which QGP signatures has been affirmed [27]. Also, pp collision performed at $\sqrt{s} = 5.02$ TeV in LHC is in agreement with our estimation $\sqrt{s}_{cL} = 3.7$ TeV.

5. Conclusions

The Color String Percolation Model exhibits finite size effects in its observables that need to be taken into account, and that can be expressed in terms of the nucleon number A_M. In particular, the transition temperature associated with the QGP formation is higher for small systems than for large ones. This implies that small systems like pp collisions require higher energy or higher multiplicity. Notice that our estimations of minimal $\sqrt{s}$ for QGP formation are consistent with those reported in the literature.

Acknowledgements

We thank Carlos Pajares for his valuable comments and fruitful discussions. D. R. H. acknowledges financial support from Consejo Nacional de Humanidades, Ciencias y Tecnologías under fellowship grant number 1140160.

1. M. Gyulassy and L. McLerran, New forms of QCD matter discovered at RHIC, *Nucl. Phys. A* **750** (2005) 30, https://doi.org/10.1016/j.nuclphysa.2004.10.034.
2. STAR Collaboration, Experimental and theoretical challenges in the search for the quark-gluon plasma: The STAR Collaboration's critical assessment of the evidence from RHIC collisions, *Nucl. Phys. A* **757** (2005) 102, https://doi.org/10.1016/j.nuclphysa.2005.03.085.
3. PHENIX Collaboration, Formation of dense partonic matter in relativistic nucleus-nucleus collisions at RHIC: Experimental evaluation by the PHENIX Collaboration, *Nucl. Phys. A* **757** (2005) 184, https://doi.org/10.1016/j.nuclphysa.2005.03.086.
4. K. Aamodt *et al*., Elliptic Flow of Charged Particles in Pb-Pb Collisions at $\sqrt{sNN}$ = 2.76 TeV, *Phys. Rev. Lett.* **105** (2010) 252302, https://doi.org/10.1103/PhysRevLett.105.252302.
5. G. Aad *et al*., Measurement of the pseudorapidity and transverse momentum dependence of the elliptic flow of charged particles in lead-lead collisions at sNN = 2.76 TeV with the ATLAS detector, *Phys. Lett. B* **707** (2012) 330, https://doi.org/10.1016/j.physletb.2011.12.056.
6. S. Chatrchyan *et al*., Centrality dependence of dihadron correlations and azimuthal anisotropy harmonics in PbPb collisions at $\sqrt{sNN}$ = 2.76 TeV, *Eur. Phys. J. C* **72** (2012) 10052, https://doi.org/10.1140/epjc/s10052-012-2012-3.
7. M. Braun *et al*., De-confinement and clustering of color sources in nuclear collisions, *Phys. Rep.* **599** (2015) 1, https://doi.org/10.1016/j.physrep.2015.09.003.
8. I. Bautista, C. Pajares, and J. E. Ramírez, String percolation in AA and p+ p collisions, *Rev. Mex. Fis.* **65** (2019) 197, https://doi.org/10.31349/RevMexFis.65.197.
9. M. A. Braun and C. Pajares, Implications of color-string percolation on multiplicities, correlations, and the transverse momentum, *Eur. Phys. J. C* **16** (2000) 349, https://doi.org/10.1007/s100520050027.
10. N. Armesto *et al.*, Percolation Approach to Quark-Gluon Plasma and J/ψ Suppression, *Phys. Rev. Lett.* **77** (1996) 3736, https://doi.org/10.1103/PhysRevLett.77.3736.
11. C. Pajares, String and parton percolation, *Eur. Phys. J. C* **43** (2005) 9, https://doi.org/10.1140/epjc/s2005-02179-y
12. M. A. Braun and C. Pajares, Transverse momentum distributions and their forward-backward correlations in the percolating color string approach, *Phys. Rev. Lett.* **85** (2000) 4864, https://doi.org/10.1103/PhysRevLett.85.4864.
13. M. Braun *et al.*, Cumulative particle production and percolation of strings, *The European Physical Journal C-Particles and Fields* **25** (2002) 249 https://doi.org/10.1007/s10052-002-0989-8.
14. J. D. De Deus and C. Pajares, Percolation of color sources and critical temperature, *Phys. Lett. B* **642** (2006) 455, https://doi.org/10.1016/j.physletb.2006.10.018.
15. I. Bautista, C. Pajares, and J. E. Ramírez, String percolation in AA and p+p collisions, *Rev. Mex. Fis.* **65** (2019) 197.
16. M. A. Braun, F. Del Moral, and C. Pajares, Percolation of strings and the relativistic energy data on multiplicity and transverse momentum distributions, *Phys. Rev. C* **65** (2002) 024907. https://doi.org/10.1103/PhysRevC.65.024907.
17. M. Braun *et al*., De-confinement and clustering of color sources in nuclear collisions, *Physics Reports* **599** (2015) 1, https://doi.org/10.1016/j.physrep.2015.09.003.
18. J. E. Ramírez, B. Díaz, and C. Pajares, Interacting color strings as the origin of the liquid behavior of the quark-gluon plasma, *Phys. Rev. D* **103** (2021) 094029, https://doi.org/10.1103/PhysRevD.103.094029.
19. M. A. Braun and C. Pajares, Transverse momentum distributions and their forward-backward correlations in the percolating color string approach, *Phys. Rev. Lett.* **85** (2000) 4864, https://doi.org/10.1103/PhysRevLett.85.4864.
20. J. E. Ramírez, A. F. Téllez, and I. Bautista, String percolation threshold for elliptically bounded systems, *Phys. A: Stat. Mech. Appl.* **488** (2017) 8, https://doi.org/10.1016/j.physa.2017.07.002.
21. M. Nardi and H. Satz, String clustering and J/ψ suppression in nuclear collisions, *Phys. Lett. B* **442** (1998) 14, https://doi.org/10.1016/S0370-2693(98)01234-9.
22. M. N. Chernodub, Kertész Line and Embedded Monopoles in QCD, *Phys. Rev. Lett.* **95** (2005) 252002, https://doi.org/10.1103/PhysRevLett.95.252002.
23. S. Mertens and C. Moore, Continuum percolation thresholds in two dimensions, *Phys. Rev. E* **86** (2012) 061109, https://doi.org/10.1103/PhysRevE.86.061109.
24. D. Stauffer and A. Aharony, Introduction To Percolation Theory (Taylor & Francis, 1994), https://doi.org/10.1201/9781315274386.
25. I. Bautista *et al.*, Multiplicity in pp and AA collisions: the same power law from energy-momentum constraints in string production, *Phys. Lett. B* **715** (2012) 230, https://doi.org/10.1016/j.physletb.2012.07.029.
26. J. C. Texca García *et al*., Percolation leads to finite-size effects on the transition temperature and center-of-mass energy required for quark-gluon plasma formation, *Phys. Rev. D* **106** (2022) L031503, https://doi.org/10.1103/PhysRevD.106.L031503.
27. A. N. Mishra *et al*., SISSA: ALICE data in the framework of the Color String Percolation Model, *PoS* **LHCP2019** (2019) 004, https://doi.org/10.22323/1.350.0004.
28. T. Biro, H. B. Nielsen, and J. Knoll, Colour rope model for extreme relativistic heavy ion collisions, *Nucl. Phys. B* **245** (1984) 449, https://doi.org/10.1016/0550-3213(84)90441-3.
29. M. E. Newman and R. M. Ziff, Fast Monte Carlo algorithm for site or bond percolation, *Phys. Rev. E* **64** (2001) 016706, https://doi.org/10.1103/PhysRevE.64.016706.
30. J. E. Ramírez and C. Pajares, Area covered by disks in smallbounded continuum percolating systems: An application to the string percolation model, *Phys. Rev. E* **100** (2019) 022123, https://doi.org/10.1103/PhysRevE.100.022123.